Microfabrication and Characterisation of an Electrostatic MEMS Energy Harvester for Biomedical Applications

Francisco Ambia, Xavier Leroux, Nathalie Isac, Elie Lefeuvre

▶ **To cite this version:**

Francisco Ambia, Xavier Leroux, Nathalie Isac, Elie Lefeuvre. Microfabrication and Characterisation of an Electrostatic MEMS Energy Harvester for Biomedical Applications. Symposium on Design, Test, Integration & Packaging of MEMS and MOEMS 2022, Jul 2022, Pont-a-Mousson, France. 10.1109/dtip56576.2022.9911722 . hal-04205064

HAL Id: hal-04205064
https://hal.science/hal-04205064

Submitted on 13 Sep 2023

HAL is a multi-disciplinary open access archive for the deposit and dissemination of scientific research documents, whether they are published or not. The documents may come from teaching and research institutions in France or abroad, or from public or private research centers.

L'archive ouverte pluridisciplinaire **HAL**, est destinée au dépôt et à la diffusion de documents scientifiques de niveau recherche, publiés ou non, émanant des établissements d'enseignement et de recherche français ou étrangers, des laboratoires publics ou privés.

2022 Symposium on Design, Test, Integration and Packaging of MEMS/MOEMS (DTIP) | 978-1-6654-9167-9/22/$31.00 ©2022 IEEE | DOI: 10.1109/DTIP56576.2022.9911722

Microfabrication and Characterisation of an Electrostatic MEMS Energy Harvester for Biomedical Applications

Francisco Ambia
Centre de Nanosciences et de Nanotechnologies
Université Paris-Saclay - CNRS, 10 boulevard Thomas Gobert, 91120 Palaiseau, France
jose-francisco.ambia-campos@universite-paris-saclay.fr

Xavier Leroux
Centre de Nanosciences et de Nanotechnologies
Université Paris-Saclay - CNRS, 10 boulevard Thomas Gobert, 91120 Palaiseau, France
xavier.leroux@universite-paris-saclay.fr

Nathalie Isac
Centre de Nanosciences et de Nanotechnologies
Université Paris-Saclay - CNRS, 10 boulevard Thomas Gobert, 91120 Palaiseau, France
nathalie.isac@ universite-paris-saclay.fr

Elie Lefeuvre
Centre de Nanosciences et de Nanotechnologies
Université Paris-Saclay - CNRS, 10 boulevard Thomas Gobert, 91120 Palaiseau, France
elie.lefeuvre@universite-paris-saclay.fr

***Abstract*—We present the fabrication process and characterization of a novel Silicon-on-Glass electrostatic MEMS vibration energy harvester. This device is aimed to give supplementary energy to the battery of leadless pacemakers by using the vibrations generated by heartbeat movement. The proposed device is compliant with Leadless Pacemakers requirements: its dimensions are compatible with the 6mm-diameter capsules of leadless pacemakers for catheterism, and the materials composing the device are not ferromagnetic, allowing MRI imaging of implanted patients.**

Keywords—Silicon on Glass, Leadless Pacemakers, MEMS, Vibration Energy Harvesting.

I. INTRODUCTION

Leadless pacemakers have important advantages over conventional pacemakers [1], they reduce the risk of complications such as pneumothorax, subclavian vein thrombosis, they reduce the risk of lead-related problems such higher surface for infection and tricuspid valve malfunction. Although leadless pacemakers bring important improvements, there are some downsides such as the reduced space for batteries due to the miniaturization of the implant. In addition, a major problem in both leadless and conventional pacemakers is premature battery depletion which increases the risk of surgical intervention [2] .

Premature battery depletion and reduced spaces for batteries make design engineers to look for supplementary sources of energy to power leadless pacemakers. Supplementary sources of energy have been explored for biomedical implants, examples are ultrasonic energy harvesters [3] and electromagnetic wireless energy transfer [4]. There are other sources of energy that allow the device to be completely autonomous by using the energy in the implant's environment, examples of such sources are electric potential gradients in the cell's membrane [5] and the motions of the heart [6].

There exist mainly three transduction mechanisms to transform mechanical energy to electrical: piezoelectric [7], electrostatic [8] and electromagnetic [9]. In the present work we focus on getting energy from the motions of the heart, we make use of this movement to make a low frequency oscillator vibrate to convert vibrations to electric power.

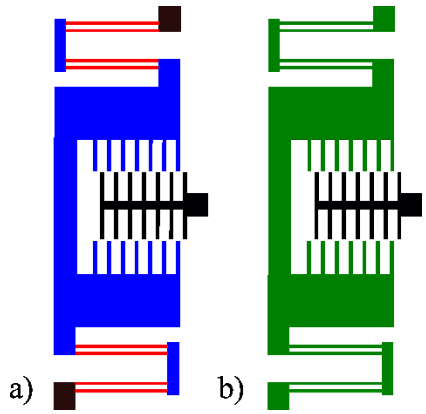

Fig. 1. Mechanical and electrical diagrams of the device.

The electrostatic MEMS transduction shows some advantages over piezoelectric and electromagnetic ones due to miniaturization possibilities, batch fabrication processes and compatibility with MRI. The electrostatic transduction consists on subjecting to vibrations a mechanical harmonic oscillator, these displacement oscillations move capacitor combs and change the capacitance of the system. By charging and discharging the variable capacitance in a synchronized fashion, one is able to transform a change in capacitance in electric power as reported in [10].

This work is the continuation of the previous work presented in [11]. We present herein an improved design which enabled to reduce the mechanical stress in the silicon springs compared to the asymmetrical former design.

978-1-6654-9167-9/22/$31.00 ©2022 IEEE

Authorized licensed use limited to: Université Paris-Saclay. Downloaded on September 12,2023 at 13:14:38 UTC from IEEE Xplore. Restrictions apply.

II. Device Structure and Design

The aspect ratio of the implant constrains the dimensions of the MEMS device, the presented device is 17.8mm long, 1.2mm thick and it has a width of 3.8mm. These dimensions allow to place two devices inside the envisioned implant. To our knowledge, this is the first energy harvesting MEMS device with this form factor.

In Figure 1, it is shown the mechanical and electrical structure of the device. In Figure 1a black elements represent fixed part that are not compliant nor moving, in blue are parts that are not compliant and moving, finally in red are compliant and moving parts. In Figure 2a black represents grounded electrodes and green represents the parts that are at some potential V.

The device is a linear oscillator coupled to a variable capacitor, the device changes capacitance when the combs engage due to oscillations of the mechanical part of the device. The vibrations are transformed into electric power by driving the device by a rectangular QV cycle as the one depicted in Figure 5.

The resonant frequency of the mechanical oscillator was chosen taking into the account the average displacement of the moving part due to gravity. Gravity induces an offset on the moving part, this offset grows as Equation (1).

$$\Delta u_{offset} = \frac{g}{2\pi f_n} \tag{1}$$

Where Δu_{offset} is the displacement due to gravity, g is gravity and f_n is the resonant frequency of the oscillator. The lower the resonant frequency, the higher the effect of gravity will be, we have to do a compromise between the offset and getting the natural frequency as low as possible to match the highest element in heart beat acceleration spectrum (around 1Hz).

The MEMS device maximum displacement is constraint by stoppers to protect the beams from breaking, the maximum displacement amplitude of the mobile part is $200\mu m$ in each side. In order to avoid sticking on one stopper due to gravity, we choose a natural frequency of 57Hz to have an offset of $76.48\mu m$ when gravity field is parallel to the direction of motion of the mobile part. This offset forbids the capacitor combs to engage and disengage completely, this causes the output power to be lower compared to the case when gravity field is perpendicular to the direction of motion [11].

The desired power output of the device is around 5µW, this estimation is the power consumption of the low power electronics of the leadless pacemaker. The MEMS device should be able to supply at least this energy even when the gravity filed is parallel to the movement.

There are two parameters to tune the resonant frequency: the mass and the spring constant. The spring constant is given by the geometry of the beams, the compliant elements in red in Figure 1. The spring constant of the overall device is given by Equation (2).

$$k_{eq} = \frac{\pi^4}{48} EW \left(\frac{H}{L}\right)^3 \tag{2}$$

Where E is the Young's Modulus of Silicon, H is the width of the beam $30\mu m$, W is the thickness of the device $200\mu m$ and L is the length of the beam $3580\mu m$.

The geometry of the device springs is different of traditional MEMS springs as the folded spring described in [12]. The design is similar to the folded spring, we use double beams to avoid contact between the combs. The double beams constraint the movements on the in plane perpendicular direction of movement by avoiding rotations of the spring arm supports. This geometry allows to distribute better the weight of the mass compared to the guiding beam design in [11].

III. Fabrication

The MEMS device was fabricated using a four-inch SOG wafer, according to the process depicted in Figure 2. First, the device design was patterned in the photoresist by photolithography. Then, $200\mu m$ depth DRIE anisotropic etching of silicon was performed to reach the glass beneath.

After DRIE, 200nm gold electrodes were deposited to get electrical contacts on the variable capacitor. The SOG wafer was then diced to separate the devices. HF (hydrofluoric acid) wet etching enabled to release the mobile parts of the silicon MEMS from the glass wafer. A SEM image of the MEMS after dicing is shown in Figure 3.

Stiction is avoided during wet HF etching thanks to the spring's high rigidity in the out of plane and in plane perpendicular directions. After HF wet etching, the device is rinsed with isopropyl alcohol to remove de HF acid, finally the device is heated to at 80°C to evaporate the alcohol. The capillarity effects are low in the level of combs because the combs are not engaged in the rest position, this leaves low curvature droplets of alcohol to evaporate without exerting strong forces between the mobile and fixed parts.

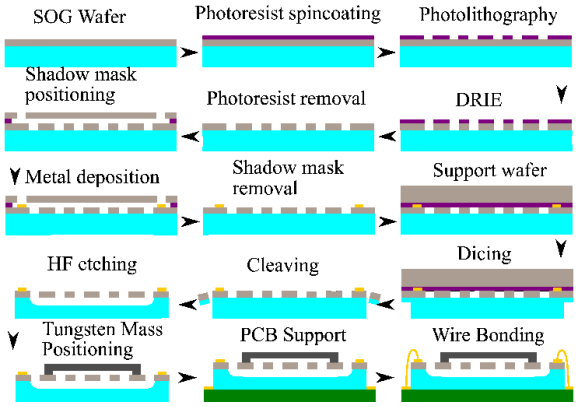

Fig. 2. Fabrication Process

A supplementary 300mg tungsten mass was bonded on top of the device. This mass helps bringing down the resonant frequency of the device to match the desired resonant low frequency of 57Hz.

The mass was placed with a pick and place robot, the mass has an inverted U shape: a bridge that connects two feet. The feet are in contact with the device, they are placed on the circles depicted in Figure 3, these circles are useful for placing the mass in a controlled position. Epoxy glue sticks the mass feet with the device.

Finally, the device was attached on a PCB and electrically connected by wire bonding. Therefore, the device could be

Authorized licensed use limited to: Université Paris-Saclay. Downloaded on September 12,2023 at 13:14:38 UTC from IEEE Xplore. Restrictions apply.

connected easily to an interface circuit such as reported in [13].

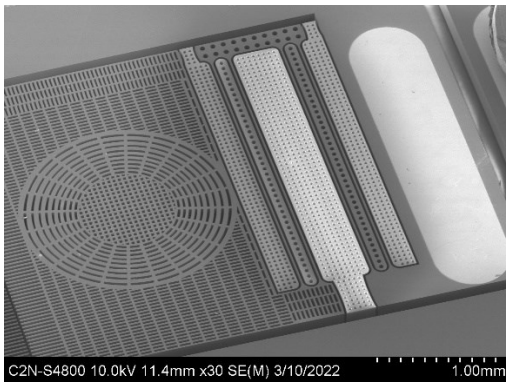

Fig. 3. SEM image of device springs before wet HF etching

IV. Characterisation

The change in capacitance of the MEMS is crucial for energy conversion. One may define an auxiliary parameter $\kappa = C_{max}/C_{min}$, C_{max} and C_{min} being respectively the maximal and minimal capacitance of the MEMS. This parameter helps to choose the most effective interface circuit for optimal electric power generation [14].

Figure 4 shows the capacitance as a function of displacement which was determined experimentally. It was found a maximal and a minimal capacitance of 69.72pF and 11.37pF respectively, meaning κ~7. For this configuration, the optimal ratio between maximum and minimal voltage is four. The closest rectangular QV cycle to this ratio is obtained using the Bennet's voltage doubler (circuit with one cell in [13]).

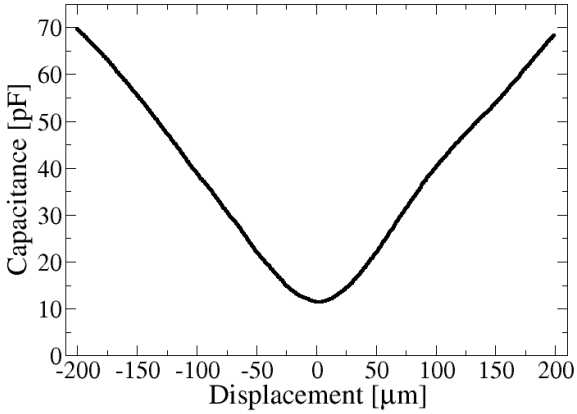

Fig. 4. Experimental capacitance variation as a function of the displacement of the mobile part.

The device was connected to a voltage doubler interface circuit depicted in Figure 7b [13]. The oscillator was excited with a sinusoidal acceleration of 0.75g amplitude at its resonant frequency. The amplitude of accelerations was chosen so that the device reaches the maximal allowed displacement of ±200µm to reach the highest change in capacitance.

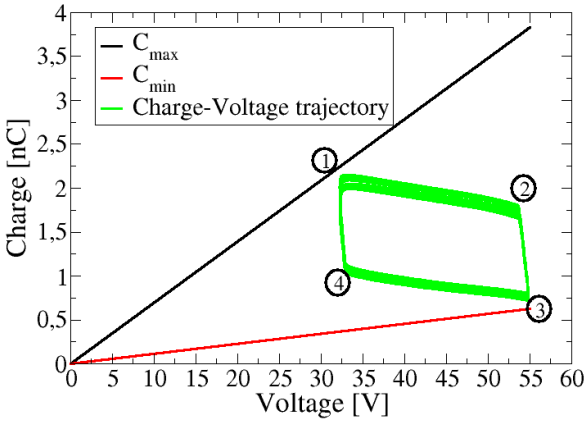

Fig. 5. Experimental QV cycle

The interface circuit drives the device to perform a rectangular charge-voltage cycle, consisting of two quasi-adiabatic voltage variations ① → ② , ③ → ④ and two charge variations at quasi-constant voltage ② → ③, ④ → ①, as shown in Figure 5.

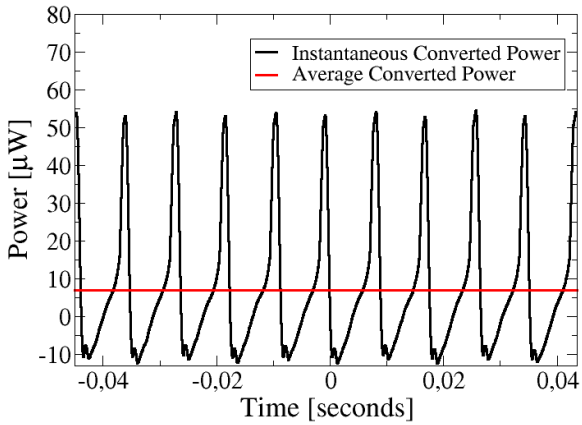

Fig. 6. Instantaneous Power

Each rectangle in Figure 5 corresponds to a complete wave cycle of the power conversion represented in Figure 6. The variable capacitor charges in ④ → ① giving a net negative instantaneous power. After mechanical work is performed by vibration in ① → ②, the capacitor is discharged in ② → ③.

In Figure 7a the Roundy charge pump is shown [10], this interface circuit drives the circuit in an ideal rectangular QV-cycle. Ideal diodes would perform true adiabatic process with no energy exchanges, ideal voltage sources would perform constant voltage process without variations of tension. In practice this cannot be done, real diodes have parasitic capacitances. The slopes in quasi-adiabatic process ① → ②, ③ → ④ appear due to the parasitic capacitances in the diodes.

The doubler circuit depicted in Figure 7b yields processes at quasi-constant voltage ② → ③, ④ → ① which are not vertical lines as in the ideal case. The voltage doubler uses capacitors to bias the variable capacitor, as the capacitance changes, the variable capacitor exchanges charge with the capacitors in the interface circuit, due to charge variations in the interface circuit, the slopes in processes ② → ③ and ④ → ① appear.

By measuring the voltage and current going through the variable capacitor, one can compute the instantaneous

Authorized licensed use limited to: Université Paris-Saclay. Downloaded on September 12,2023 at 13:14:38 UTC from IEEE Xplore. Restrictions apply.

converted power depicted in Figure 6. The discharge corresponds to the positive power peaks depicted in Figure 6. Averaging the instantaneous power yields a net positive power of 7µW, shown as the red line in Figure 6.

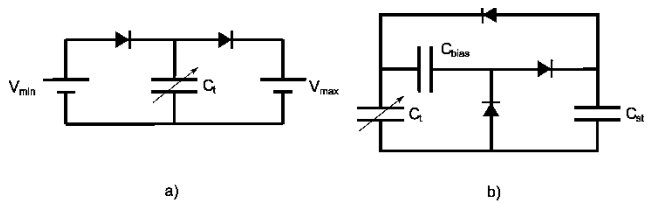

Fig. 7. SEM Circuit interfaces for electrostatic vibration energy harvesters.

The discharge corresponds to the positive power peaks depicted in Figure 6. Averaging the instantaneous power yields a net positive power of 7µW, shown as the red line in Figure 6.

V. CONCLUSIONS

The fabrication and characterization of an electrostatic MEMS energy harvester designed for medical implant application was presented. Despite severe constraints in terms of shape to enable implantation through catheterization, the device exhibited excellent performances in terms of generated power. Experimental results confirm thus that the presented device is a promising candidate to power the next generation leadless pacemakers. Ongoing ex-vivo analysis using cardiac acceleration signals will help to assess the device performances in realistic operating conditions, making then possible to envision acute and chronic pre-clinical tests.

REFERENCES

[1] J. Z. Lee, S. K. Mulpuru, and W. K. Shen, "Leadless pacemaker: performance and complications," *Trends Cardiovasc. Med.*, vol. 28, no. 2, pp. 130–141, 2018.

[2] A. S. Manolis, T. Maounis, S. Koulouris, and V. Vassilikos, "'Real life' longevity of implantable cardioverter-defibrillator devices," *Clin. Cardiol.*, vol. 40, no. 9, pp. 759–764, 2017.

[3] Q. Shi, T. Wang, and C. Lee, "MEMS based broadband piezoelectric ultrasonic energy harvester (PUEH) for enabling self-powered implantable biomedical devices," *Sci. Rep.*, vol. 6, no. 1, pp. 1–10, 2016.

[4] G. Xu, X. Yang, Q. Yang, J. Zhao, and Y. Li, "Design on magnetic coupling resonance wireless energy transmission and monitoring system for implanted devices," *IEEE Trans. Appl. Supercond.*, vol. 26, no. 4, pp. 1–4, 2016.

[5] L. Catacuzzeno, F. Orfei, A. Di Michele, L. Sforna, F. Franciolini, and L. Gammaitoni, "Energy harvesting from a bio cell," *Nano Energy*, vol. 56, pp. 823–827, 2019.

[6] C. Dagdeviren *et al.*, "Conformal piezoelectric energy harvesting and storage from motions of the heart, lung, and diaphragm," *Proc. Natl. Acad. Sci.*, vol. 111, no. 5, pp. 1927–1932, 2014.

[7] E. Lefeuvre, G. Sebald, D. Guyomar, M. Lallart, and C. Richard, "Materials, structures and power interfaces for efficient piezoelectric energy harvesting," *J. Electroceramics*, vol. 22, no. 1, pp. 171–179, 2009.

[8] V. Dorzhiev, A. Karami, P. Basset, F. Marty, V. Dragunov, and D. Galayko, "Electret-free micromachined silicon electrostatic vibration energy harvester with the Bennet's doubler as conditioning circuit," *IEEE Electron Device Lett.*, vol. 36, no. 2, pp. 183–185, 2015.

[9] B. Yang *et al.*, "Electromagnetic energy harvesting from vibrations of multiple frequencies," *J. Micromechanics Microengineering*, vol. 19, no. 3, p. 035001, 2009.

[10] S. Roundy, P. K. Wright, and K. S. Pister, "Micro-electrostatic vibration-to-electricity converters," in *ASME international mechanical engineering congress and exposition*, 2002, vol. 36428, pp. 487–496.

[11] F. Ambia, J. Chavez, M. Lallart, X. Leroux, and E. Lefeuvre, "Design and Simulation of an Electrostatic Energy Harvester for Biomedical Implants," in *2021 Symposium on Design, Test, Integration & Packaging of MEMS and MOEMS (DTIP)*, 2021, pp. 1–6.

[12] S. D. Senturia, *Microsystem design*. Springer Science & Business Media, 2007.

[13] E. Lefeuvre, S. Risquez, J. Wei, M. Woytasik, and F. Parrain, "Self-biased inductor-less interface circuit for electret-free electrostatic energy harvesters," in *Journal of Physics: Conference Series*, 2014, vol. 557, no. 1, p. 012052.

[14] D. Galayko *et al.*, "Capacitive energy conversion with circuits implementing a rectangular charge-voltage cycle—part 1: Analysis of the electrical domain," *IEEE Trans. Circuits Syst. Regul. Pap.*, vol. 62, no. 11, pp. 2652–2663, 2015.

Authorized licensed use limited to: Université Paris-Saclay. Downloaded on September 12,2023 at 13:14:38 UTC from IEEE Xplore. Restrictions apply.